Electronic Supplementary Material (ESI) for ChemComm.


# Nickel cobalt oxide hollow nanosponges as advanced electrocatalysts for the oxygen evolution reaction

**Chengzhou Zhu,[a] Dan Wen,[a] Susanne Leubner,[a] Martin Oschatz,[b] Wei Liu,[a] Matthias Holzschuh,[a] Frank Simon,[c] Stefan Kaskel,[b] and Alexander Eychmüller[a]***

## EXPERIMENTAL SECTION

**Chemicals:** $NiCl_2.6H_2O$ and $CoCl_2.6H_2O$ were purchased from Sigma and used as received without further purification. Commercial Pt/C (20wt%) catalyst was purchased from Alfa Aesar. NaBH4 were obtained from Aldrich. Unless otherwise stated, other reagents were of analytical grade and were used as received. All aqueous solutions were prepared with ultrapure water (>18 MΩ) from a Milli-Q Plus system (Millipore).

**Apparatus:** TEM measurements were made on an EM 208S with an accelerating voltage of 100 kV. X-ray powder diffraction (XRD) was carried out on Siemens D5000 X-ray diffractometer using Cu Kα (1.5406 Å) radiation. Scanning electron microscopy (SEM) was performed on a Zeiss DSM 982 Gemini instrument. Thermogravimetry analysis (TGA) was measured on METTLER TOLEDO TGA/DSC1 STRAe System under an argon flow of about 30 mL/min in the temperature range of 25 °C-600 °C at a heating rate of 2 °C/min. The sample was put in standard 70 μL $\alpha$-$Al_2O_3$ crucible. Inductively coupled plasma optical emission spectroscopy (ICP-OES) was carried out on Perkin-Elmer Optima 7000DV optical emission spectrometer. Nitrogen physisorption isotherms were measured at 77 K on a Quantachrome Autosorb 1C instrument. Prior to the measurement, the samples were degassed in vacuum at 323 K for 24 h. The specific surface area was calculated by using multipoint Brunauer-Emmett-Teller (BET) equation ($0.05<P/P_o<0.2$), and the pore size distribution was determined from the isotherm using quenched solid density functional theory (QSDFT) equilibrium model based on a slit shaped pore geometry (carbon surface). Micropore volumes were calculated from the cumulative pore

volumes at a diameter of 2 nm. The Barrett−Joyner−Halenda (BJH) pore size distributions were calculated from the desorption braches of the isotherms. Since BJH theory underestimates the sizes of small to medium mesopores, the carbon based QSDFT model has been chosen here. Electrochemical experiments (Cyclic voltammetry and linear sweep voltammetry) were performed on an Autolab/PGSTAT 30 (Eco Chemie B. V. Utrecht, the Netherlands) in an earthed Faraday cage. A conventional three electrode cell was used, including an Ag/AgCl electrode as reference electrode, a platinum foil as counter electrode, and the modified glassy carbon electrode (GCE, 3 mm in diameter) as working electrode.

**Preparation of ternary nickel cobalt oxide hollow nanosponges.** Bimetallic Ni-Co nanosponges were first synthesized via a simple method. In a typical synthesis, 6 mL of the metal precursors containing 4.0 mL $CoCl_2$ (0.1 M) solution and 2.0 mL $NiCl_2$ (0.1 M) solution was quickly injected into 30 mL of an aqueous solution of 0.1 M $NaBH_4$ with stirring. Bimetallic porous nanostructures could be formed accompanying by the release of hydrogen. The stirring was continued for about 5 min until the entire solution became colorless. After supercritical dry, the Bimetallic Ni-$Co_2$ nanosponges were annealed in air at 600 °C for 2 h with a heating rate of 2 °C $min^{-1}$. Furthermore, we varied the mole ratios of Co and Ni sources in the precursor solutions to prepare nickel cobalt oxide hollow nanosponges with different mole ratios. As such, nickel and its derived oxide nanosponges could be also obtained through the same way mentioned above. Furthermore, monometallic cobalt and their oxide nanoparticles were also prepared using this method.

**Electrocatalytic experiments**. Prior to the surface coating, the GCE was polished carefully with 1.0, 0.3 and 0.05 μm alumina powder, respectively, and rinsed with deionized water, followed by sonicated in acetone and doubly distilled water successively. Then, the electrode was allowed to

dry under nitrogen. Nickel cobalt oxides catalyst aqueous solution was dropped on the surface of GCE and dried. The loading of catalyst on the GCE was limited to 0.2 mg $cm^{-2}$. Then, 5 μL of Nafion (0.2 %) was placed on the surface of the above materials modified GCE and dried before electrochemical experiments. The ohmic potential drop (iR) losses that arise from the solution resistance were all corrected through the EIS technique. Note that the current density was normalized to the geometrical area and the measured potentials vs Ag/AgCl were converted to a reversible hydrogen electrode (RHE) scale according to the Nernst equation ($E_{RHE} = E_{Ag/AgCl}$ +0.059 pH + 0.197); the overpotential (η) was calculated according to the following formula: η (V) = $E_{RHE}$ -1.23 V.

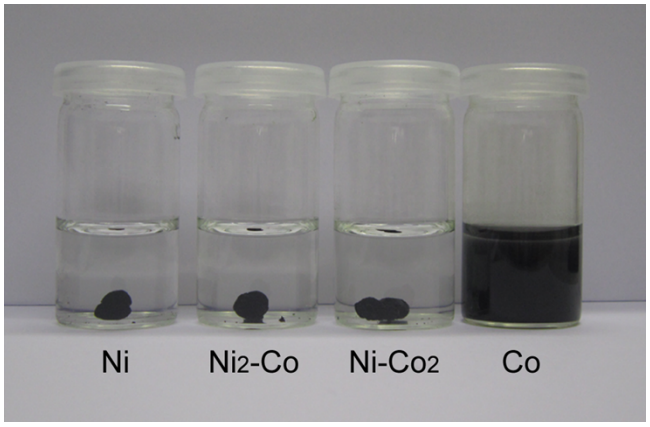


Figure S1. Digital photographs of the monometallic Ni nanosponges, bimetallic $Ni_2$-Co and Ni-$Co_2$ nanosponges and monometallic Co nanoparticles.

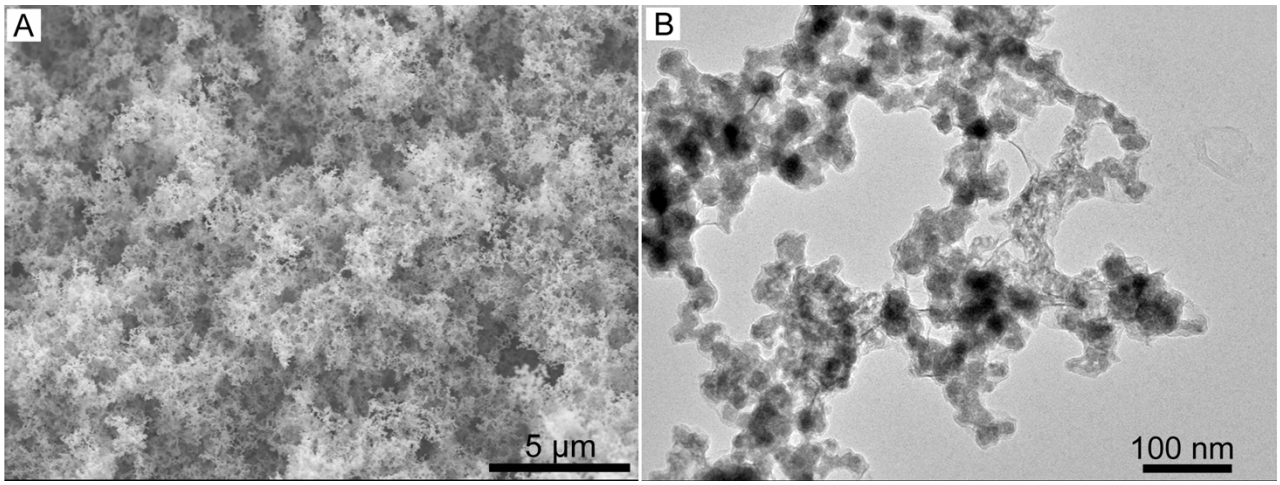


Figure S2. (A) SEM and (B) TEM images of the bimetallic Ni-$Co_2$ nanosponges.

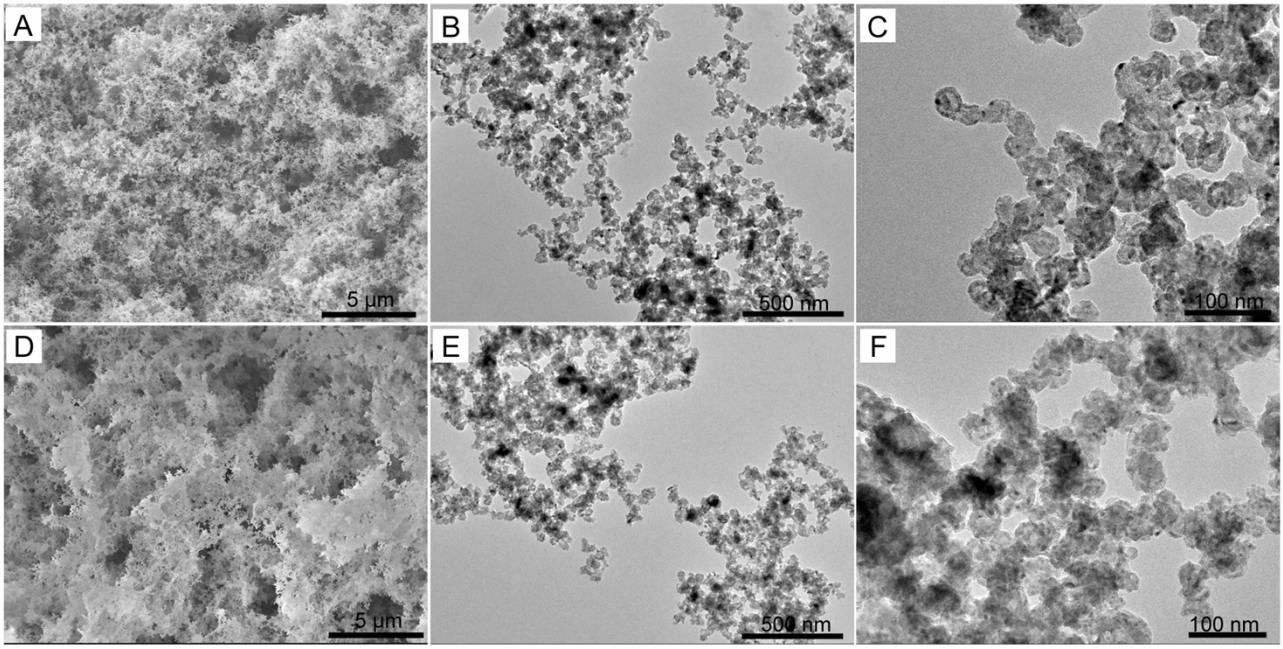


Figure S3. (A,D) SEM and (B, C, E and F) TEM images of the as-obtained NiO (A-C) and $Ni_2$-Co-O (D-F) HNSs.

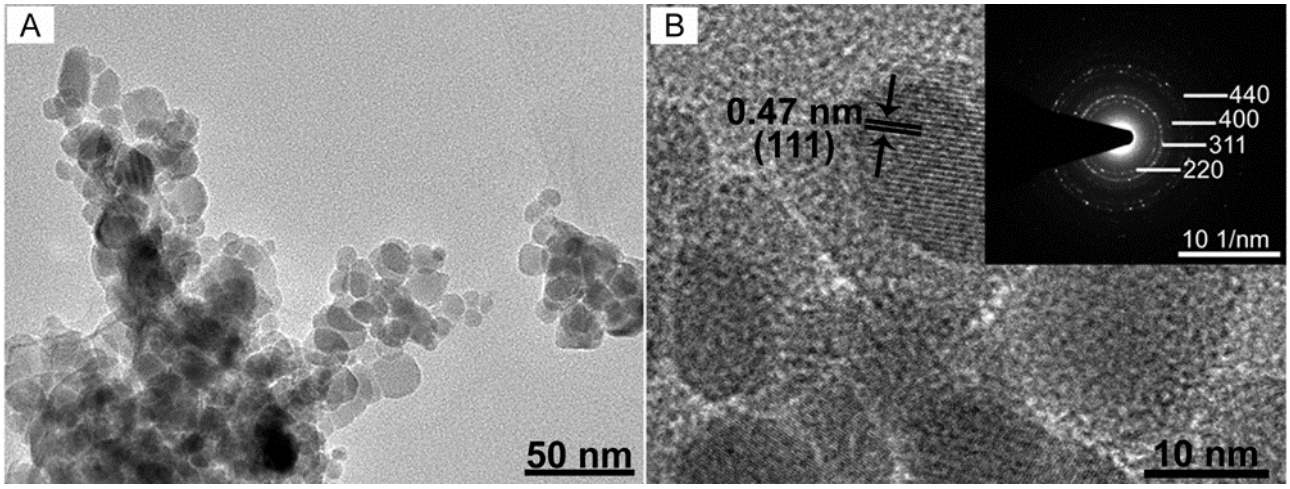


Figure S4. TEM (A) and HRTEM (B) images of $Co_3O_4$ nanoparticles. Inset shows the SAED pattern.

As a control, only Co nanoparticles precipitate rather than 3D nanosponges were obtained using this kinetically controlling reduction method. Furthermore, no hollow nanostructures were found within derived $Co_3O_4$ after annealing (Figure S4A). A HRTEM was carried out to illustrate the detailed features. As shown in Figure S4B, the lattice fringes can be readily indexed to the (111) crystal plane of the $Co_3O_4$ phase. In addition, the corresponding SAED pattern (the inset in Figure S4B) indicates the polycrystalline nature of this product, and the diffraction rings can be readily indexed to the (220), (311), (400), and (440) planes of the $Co_3O_4$ phase.

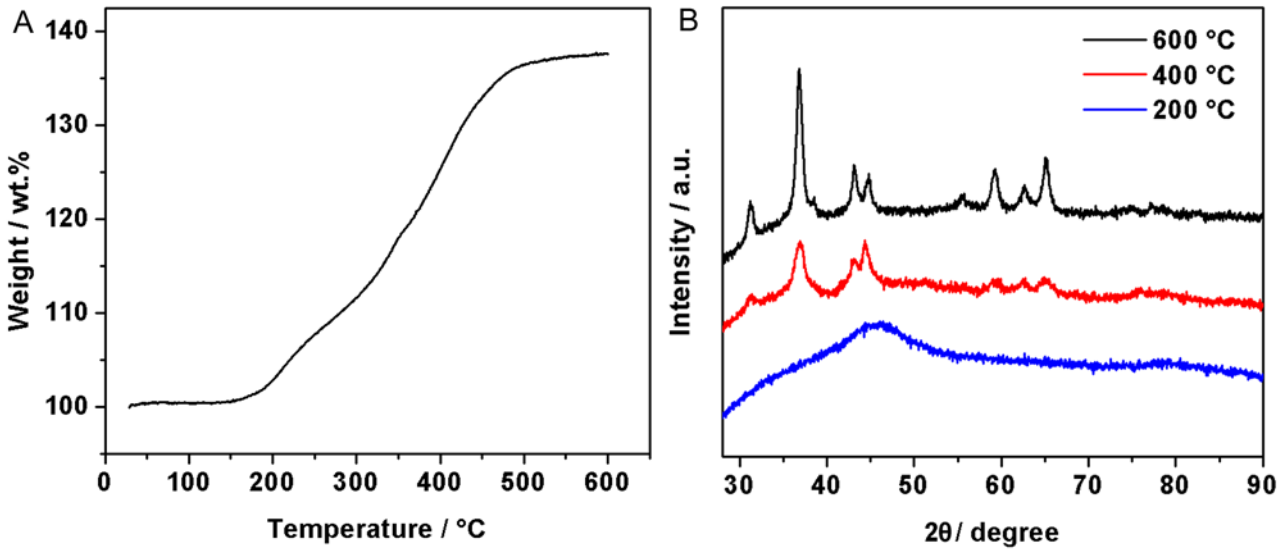


Figure S5. (A) The TGA curve of the as-prepared Ni-$Co_2$ nanosponges at a heating rate of 2 °C $min^{-1}$ in air atmosphere. (B) XRD patterns of the Ni-$Co_2$ nanosponges annealed at different temperatures.

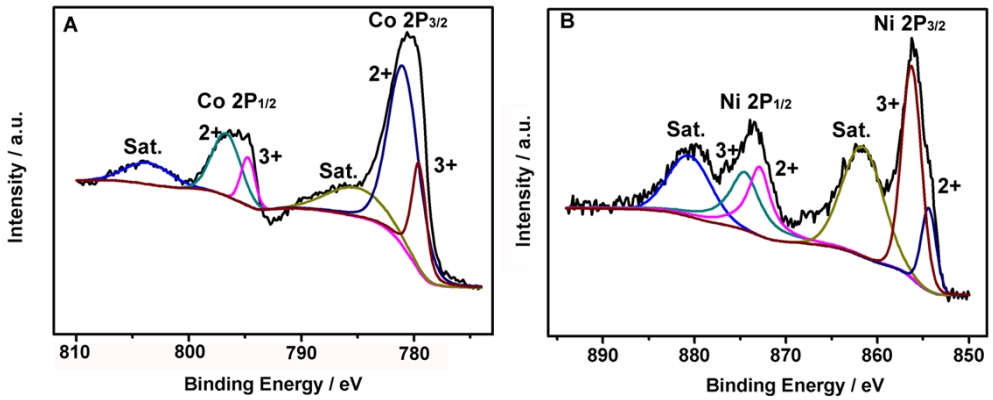


Figure S6. High-resolution Co2p (A) and Ni2p (B) XPS spectra for Ni-$Co_2$-O HNSs.

By using a Gaussian fitting method, the Co 2p emission spectrum (Figure S6A) was best fitted with two spin-orbit doublets, characteristic of $Co^{2+}$ and $Co^{3+}$ , and two shakeup satellite (indicated as "Sat."). The binding energy at 779.5 eV and 794.7 eV are ascribed to $Co^{3+}$. Another two fitting peaks at 780.9 eV and 796.6 eV are ascribed to $Co^{2+}$. The Ni 2p was also fitted with

two spin-orbit doublets (Figure S6B), characteristic of $Ni^{2+}$ and $Ni^{3+}$, and two shakeup satellites. The fitting peaks at 854.4 eV and 872.9 eV are indexed to $Ni^{2+}$, while the fitting peaks at 856.2 eV and 874.5 eV are related to $Ni^{3+}$. These data show that the surface of the as-prepared Ni-$Co_2$-O has a composition containing $Co^{2+}$ , $Co^{3+}$ , $Ni^{2+}$ , and $Ni^{3+}$.

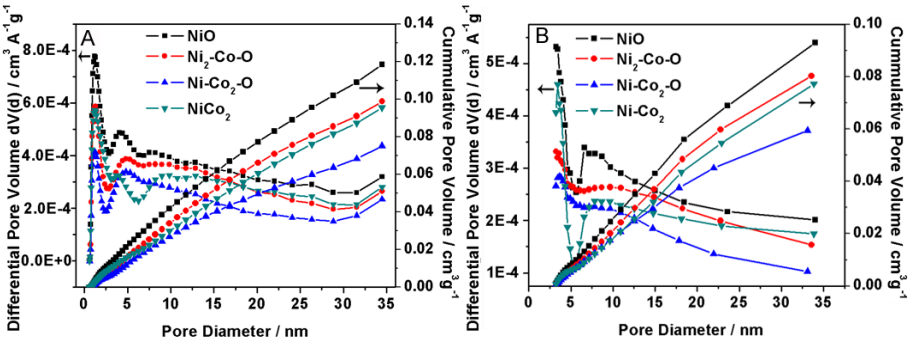


Figure S7. (A) Pore size distribution and the corresponding cumulative pore volumes for these products determined from the isotherm using quenched solid density functional theory (QSDFT) equilibrium model. (B) Pore size distribution and the corresponding cumulative pore volumes for the NiO, $Ni_2$-Co-O, Ni-$Co_2$-O and Ni-$Co_2$ nanosponges calculated from the desorption branch of the isotherm applying BJH theory.

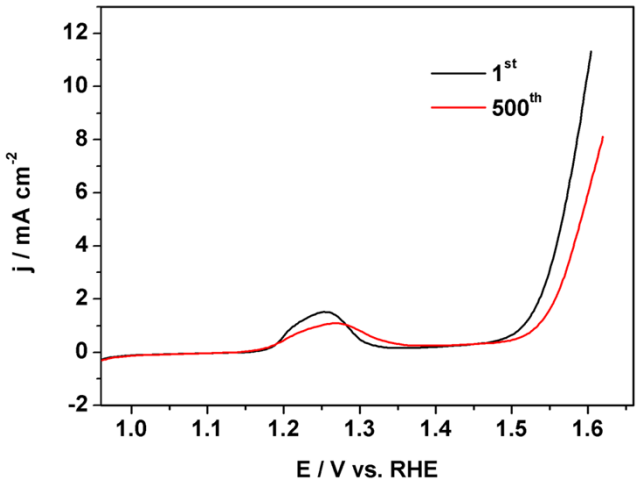


Figure S8. LSV curves for Ni-$Co_2$-O HNSs before and after CV testing of 500 cycles.

Table S1. Molar ratio of Co/Ni in the HNSs obtained EDS, ICP-OES and XPS.

| Sample | Expected Co/Ni | EDS Co/Ni | ICP-OES Co/Ni | XPS Co/Ni |
|---|---|---|---|---|
| Ni-$Co_2$-O | 67/33 | 68/32 | 67/33 | 70/30 |
| $Ni_2$-Co-O | 33/67 | 33/67 | 33/67 | 35/65 |

Table S2. Surface area and porosity of the obtained bimetallic and oxide nanosponges obtained from $N_2$ physisorption isothermal analyses.

| Samples | BET surface area [$m^2/g$] | Pore volume [$cm^3/g$] | Micropore volume [$cm^3/g$] |
|---|---|---|---|
| NiO | 43.6 | 0.309 | 0.0084 |
| $Ni_2$-Co-O | 34.4 | 0.25 | 0.0061 |
| Ni-$Co_2$-O | 24.8 | 0.216 | 0.0043 |
| Ni-$Co_2$ | 32.4 | 0.261 | 0.0065 |

Table S3. Electrochemical parameters for OER on Ni-$Co_2$-O, NiO, $Ni_2$-Co-O hollow nanosponges, $Co_3O_4$ nanoparticles, commercial Pt/C and $RuO_2$ in $O_2$-saturated 0.1 M KOH (pH ~13).

| Sample | $E_{onset}$ vs. RHE [V] | $\eta_{onset}$ [V] | j at 1.6 V vs. RHE [mA $cm^{-2}$] | η at j = 10 mA $cm^{-2}$ [V] | Tafel slope [mV/dec] |
|---|---|---|---|---|---|
| Ni-$Co_2$-O | 1.501 | 0.271 | 11.50 | 0.362 | 64.4 |
| $Co_3O_4$ | 1.555 | 0.325 | 2.94 | 0.426 | 73.2 |
| NiO | 1.593 | 0.363 | 1.74 | 0.427 | 117 |
| $Ni_2$-Co-O | 1.521 | 0.291 | 6.72 | 0.410 | 71.2 |
| Pt/C | 1.622 | 0.392 | 0.43 | - | 125.0 |
| $RuO_2$ | 1.492 | 0.262 | 6.40 | 0.413 | 82.9 |

Table S4. Electrocatalytic water oxidation properties for other reported nanomaterials.

| Catalysts | $E_{onset}$ vs. RHE [V] | η at j＝10 mA $cm^{-2}$ [V] | Tafel slope [mV/dec] | reference |
|---|---|---|---|---|
| Ni-$Co_2$-O | 1.501 | 0.362 | 64.4 | This work |
| Carbon–Cobalt-Oxide Hybrid | - | ~0.517 | - | *Chem. Eur. J.* **2014***, 20,* 4217–4221 |
| $Mn_3O_4$/$CoSe_2$ | - | 0.45 | 49 | *J. Am. Chem. Soc.* **2012**, *134*, 2930−2933 |
| $Co_3O_4$/mMWCNT | 1.51 | 0.39 | - | *J. Mater. Chem. A* **2013**, *1*, 12053-12059 |
| $CoFe_2O_4$/graphene | 1.504 | ~0.464 | - | *J. Power Sources* **2014**, *250*, 196-203 |
| Ni foam/porous carbon/anodized Ni | 1.524 | ~0.534 | - | *Angew. Chem. Int. Ed.* **2013**, 52, 5248 –5253 |
| $Co_3O_4$−$CuCo_2O_4$ | - | 0.498 | - | *Chem. Mater.* **2013**, *25*, 4926−4935 |
| $MnCo_2O_4$ | 1.564 | ~0.484 | - | *J. Electrochem. Soc.* **2014**, *161*, H296-H300 |
| $LiCoO_2$ | 1.55 | - | 52 | *Nat. Commun.* **2014**, *5*, 3949. |
| $NiCo_2O_4$ | 1.567 | ~0.412 | - | *J. Mater. Chem. A* **2013**, *1*, 12170-12177 |
| $NiCo_2O_4$–graphene | 1.558 | ~0.458 | 161 | *J. Mater. Chem. A* **2013**, *1*, 4754-4762 |

| | | | | |
|---|---|---|---|---|
| $NiCo_2S4$@N/S-doped graphene | - | 0.47 | - | *ACS Appl. Mater. Interfaces* **2013**, *5*, 5002-5008 |
| $NiCo_2O_4$ | - | 0.39 | 87 | *Nanoscale*, **2014**, *6*, 3173-3181 |
| Ni-doped $Co_3O_4$ | - | ~0.53 | - | *Chem. Commun.* **2013**, *49*, 7522 |
| porous N-doped grapheneNi$Co_2O_4$ | 1.277 | ~0.437 | 156 | *ACS Nano* **2013**, *7*, 10190-10196. |
| Nitrogen-doped carbon | - | 0.38 | - | *Nat. Commun.* **2013**, *4,* 2390. |
| Commercial $IrO_2$/C (20 wt%) | - | 0.37 | - | *Nat. Commun.* **2013**, *4,* 2390 |